Supporting Information

Van Dorp and De Zeeuw 10.1073/pnas.1314219111

SI Materials and Methods

Slice Preparation. Parasagittal slices (250 μm) where prepared from the cerebellar vermis of C57BL/6 mice, 5–7 wk old. The animals where anesthetized by isoflurane inhalation, after which the cerebellum was quickly removed and mounted in a vibratome (Leica VT1000S; Leica Microsystems). Thin sections (250 μm) were cut using a ceramic blade (Campden Instruments) in ice-cold bicarbonate-buffered solution containing (in mM) the following: 90 NaCl, 2.5 KCl, 1.25 NaH_2PO_4, 26 $NaHCO_3$, 0.5 $CaCl_2$, 4 $MgCl_2$, 25 D-glucose, 75 sucrose, and 1 kynurenic acid [bubbled with 95% (vol/vol) O_2, 5% (vol/vol) CO_2]. After cutting, slices were allowed to recover for 1 h in an artificial cerebrospinal fluid (ACSF) at 34 °C containing (in mM) the following: 127 NaCl, 2.5 KCl, 1.25 NaH_2PO_4, 26 $NaHCO_3$, 1.5 $CaCl_2$, 1 $MgSO_4$, and 20 D-glucose [bubbled with 95% (vol/vol) O_2, 5% (vol/vol) CO_2]. Slices where then stored in ACSF at room temperature for up to 6 h.

Electrophysiology. Slices were transferred to a perfusion chamber in an upright microscope (modified Olympus BX51) with infrared differential interference contrast (IR-DIC) optics and whole-field epifluorescence imaging (LaVision Biotec). Slices were continuously perfused with bubbled ACSF (2 mL/min) at room temperature (22−24 °C). ACSF was supplemented with 100 μM picrotoxin and 1 μM strychnine to block GABAergic and glycinergic inhibition. Current-clamp recordings were performed in the presence of 1 mM kynurenic acid or a mixture of 100 μM D-APV and 20 μM CNQX to block excitatory synaptic transmission. Cells in lobule IX or X were visualized with a 40× water immersed objective (Olympus LUMPLFLN) and a CCD camera (AxioCam MRm with AxioScop software; Carl Zeiss). Patch pipettes were pulled from filamented borosilicate glass capillaries (Warner Instruments) with a horizontal puller (Sutter Instruments P-97), resulting in a typical resistance of 7–8 MΩ. For current-clamp recordings (21 cells) and a subset of the voltage-clamp recordings (15 cells), pipettes were filled with a potassium-based intracellular solution containing (in mM): 140 K-gluconate, 0.2 EGTA, 10 Hepes, 4 Na_2ATP, 0.4 Na_3GTP, and 2 $MgCl_2$ (290 mOsm, pH 7.3 set with KOH). For other voltage-clamp recordings (seven cells) a cesium-based intracellular solution was used containing the following (in mM): 140 $CsMeSO_3$, 1 EGTA, 10 Hepes, 4 Na_2ATP, 0.4 Na_3GTP, 2 $MgCl_2$, 0.2 $CaCl_2$, 1 QX-314, and 1 TEA-Cl (290 mOsm, pH 7.3 set with CsOH). Unipolar brush cells (UBCs) were visually identified by their typical soma size, and morphology was confirmed in several experiments by supplementing the intracellular solution with a fluorescent dye (20 μM Alexa-Fluor 488; Invitrogen). As a reference electrode, an Ag/AgCl wire was connected to the bath through an agarose salt bridge. Whole-cell patch-clamp recordings were performed using an Axon Multiclamp 700B amplifier (Molecular Devices), and data were sampled through an Axon Digidata 1440 in combination with pClamp acquisition software (Molecular Devices) or through an onboard PCI card (NI PCI-6259; National Instruments) controlled by custom MATLAB routines (MathWorks). Signals were sampled at 20 or 50 kHz and filtered at 10 kHz. The holding potential during voltage-clamp recordings was −80 mV (unless stated otherwise). Potentials were corrected for liquid junction potential (−10 mV). The identity of UBCs could be confirmed by their whole-cell capacitance ($C_m = 17 \pm 1$ pF) and passive membrane resistance ($R_m = 652 \pm 42$ MΩ). Access resistance ($R_a = 25 \pm 1$ MΩ) was compensated ∼60%. Stocks of D-APV and CNQX (Tocris Bioscience) were prepared in water, and stocks of picrotoxin and strychnine (Sigma-Aldrich) were prepared in DMSO. These drugs were stored in aliquots at −20 °C. Kynurenic acid (Sigma-Aldrich) was dissolved in equimolar NaOH and stored at 4 °C. The final concentration of DMSO in the extracellular solution did not exceed 0.1%.

Electrical Stimulation. Current pulses were generated by an isolated pulse stimulator (A.M.P.I.) and delivered to the tissue through a double or single barrel borosilicate glass pipette. Pipettes were filled with Hepes-buffered ACSF and placed to evoke a reliable synaptic response from the white matter or granular layer. Trigger pulses were generated from an onboard PCI card (NI PCI-6259; National Instruments) controlled by custom MATLAB routines. For irregular stimulus sequences, ISIs were drawn from exponential distributions. When possible, at the end of a stimulation experiment, 20 μM CNQX and 50 μM D-APV were bath applied to confirm the synaptic nature of the response.

Data Analysis. Data were analyzed with custom MATLAB scripts (MathWorks). For analysis of fast excitatory postsynaptic currents (EPSCs), traces were low-pass filtered at 2 kHz and subsequently resampled at 5 kHz. For analysis of the slower elements of the EPSC, traces were low-pass filtered at 500 Hz and subsequently resampled at 1 kHz. The current baseline and noise SD were determined from a 1-s window before the start of a stimulus protocol. The peak of an EPSC after stimulation was determined in a 5-ms window from the start of the stimulus artifact, by taking the average of data that fell within 2 SDs of the maximal current within in the 5-ms window. A single exponential function was then fitted to the data within the first 20 ms after the peak to estimate the fast EPSC decay time. EPSC rise time was determined within a 20−80% peak amplitude window. The decay time of the slow tail was determined by fitting an exponential function to the portion below 80% of the maximum slow current. During stimulus trains, a linear function was fitted to data within 20 ms just before a stimulation artifact, to estimate the baseline amplitude and slope at the moment of stimulation. This procedure allowed for calculating the fast EPSC amplitude and rise time during stimulus trains. In some cases, the current level at the end of a long stimulation trace did not recover completely to the baseline as it was before the start of stimulation, but the difference was never larger than 4 pA and usually less than 2 pA for the cells used in this work. In these cases, a linear correction to the baseline was applied. The results of the automated analysis routines were always checked by eye afterward.

For sinusoidal current injections I_{sin}, instantaneous firing rates R were calculated as the reciprocal of the interval between successive spikes and assigned to the time in the center between two spikes. R vs. I_{sin} data were fitted to a linear function $R = GI_{sin} + B$, by minimizing the mean squared difference. The slope G provided the gain value and B was the baseline. To obtain the response phase, a sinusoidal function $R = G\sin(2\pi ft + \phi) + B$ was fitted to the responses by minimizing the mean squared difference. The frequency f was set to the modulation frequency, and gain G and baseline B were previously determined from the linear R vs. I fit. The phase ϕ of the response with respect to the input signal then followed from the sinusoidal fit; positive values indicate a phase lead. This method provided good fits, but can only be used when phase differences between input and output signals are small.

Model and Simulations. The kinetic AMPA receptor (AMPAR) model was taken from Raman and Trussell (1) and used here to simulate the fraction of open channels in a collection of AMPARs. The model was implemented in NEURON (2), and simulations were performed in Python (3, 4). The transition rates were (in ms^{-1}) as follows: $C_0 \rightleftharpoons C_1(30\ mM^{-1},\ 0.3)$, $C_1 \rightleftharpoons C_2(20\ mM^{-1},\ 600)$, $D_1 \rightleftharpoons D_2(20\ mM^{-1},\ 1.038)$, $D_2 \rightleftharpoons C_3(3.33\ mM^{-1},\ 0.22)$, $C_2 \rightleftharpoons O_2^s(3,\ 0.35)$, $C_2 \rightleftharpoons O_2^f(60,\ 3)$, $C_1 \rightleftharpoons D_1(1, 0.3)$, $C_2 \rightleftharpoons D_2(27, 0.014)$, $C_2 \rightleftharpoons O_2^f(60,\ 3)$, and $C_3 \rightleftharpoons O_3(0.006, 2)$. Rates are specified as (forward, backward). States O_2^s, O_s^f, and O_3 were summed to determine the total fraction of open channels. Transitions $C_0 \rightleftharpoons C_1$, $C_1 \rightleftharpoons C_2$, $D_1 \rightleftharpoons D_2$, and $D_2 \rightleftharpoons C_3$ were multiplied by the glutamate concentration. The bell-shaped dose–response curve of this model is due to the $D_2 \rightleftharpoons C_3$ transition and is thought to underlie biphasic EPSCs. The $C_3 \rightleftharpoons O_3$ transition is responsible for the persistent open state of the channel at high glutamate concentrations.

$$\begin{array}{ccccccc} & & & & O_2^f & & \\ & & & & \Downarrow\Uparrow & & \\ C_0 & \rightleftharpoons & C_1 & \rightleftharpoons & C_2 & \rightleftharpoons & O_2^s \\ & & \Downarrow\Uparrow & & \Downarrow\Uparrow & & \\ & & D_1 & \rightleftharpoons & D_2 & \rightleftharpoons & C_3 \\ & & & & & & \Downarrow\Uparrow \\ & & & & & & O_3 \end{array}$$

To simulate the fast EPSC peak, an instantaneous glutamate pulse was used with a 4-mM amplitude and a 0.15-ms decay time constant. Analysis based on fitting model parameters to data (Fig. 4*D*) was very insensitive to the fast glutamate peak; increasing the amplitude to 6 mM gave identical results. The slow glutamate tail was modeled as an instantaneously released quantity that decayed biexponentially. The glutamate concentration G_{slow} was thus given by

$$G_{slow} = Q_1 e^{-t/\tau_1} + Q_2 e^{-t/\tau_2}. \quad \textbf{[S1]}$$

Here Q_1 and Q_2 are glutamate release quantities, and τ_1 and τ_2 are decay time constants. To calculate the glutamate concentrations just before a stimulus within a stimulus train, the glutamate summation can be expressed as

$$G_{base}(N) = \sum_{n=2}^{N} Q_1 e^{-(n-1)T/\tau_1} + Q_2 e^{-(n-1)T/\tau_2}, \quad \textbf{[S2]}$$

for the Nth stimulus in the train, where $G_{base}(1) = 0$. T is the interstimulus interval. The steady-state approximation was obtained in the limit to very large N as

$$\lim_{N\to\infty} G_{base} = \frac{Q_1}{e^{T/\tau_1} - 1} + \frac{Q_2}{e^{T/\tau_2} - 1}. \quad \textbf{[S3]}$$

By making use of the steady-state dose–response relation of the AMPAR model, the steady-state open probability P_o can be expressed as an instantaneous function of the glutamate concentration G_{base}, that is $P_{base} = P_{base}(G_{base})$. The peak open probablity of the fast EPSC can also be related to G_{base} in the same way. Model parameters were thus Q_1, Q_2, τ_1, τ_2, and A_{base}, which was a factor to convert open probability to current (pA). Parameter values were abstracted by fitting P_{base} to experimental data of EPSC baseline adaptation in the least-square sense, using the function lsqcurvefit in MATLAB (MathWorks).

1. Raman IM, Trussell LO (1995) The mechanism of alpha-amino-3-hydroxy-5-methyl-4-isoxazolepropionate receptor desensitization after removal of glutamate. *Biophys J* 68(1):137–146.
2. Hines ML, Carnevale NT (1997) The NEURON simulation environment. *Neural Comput* 9(6):1179–1209.
3. Van Rossum G, Drake FL, eds (2001) *Python Reference Manual* (PythonLabs, Falls Church, VA). Available at www.python.org. Accessed July 28, 2013.
4. Hines ML, Davison AP, Muller E (2009) NEURON and Python. *Front Neuroinform* 3:1.

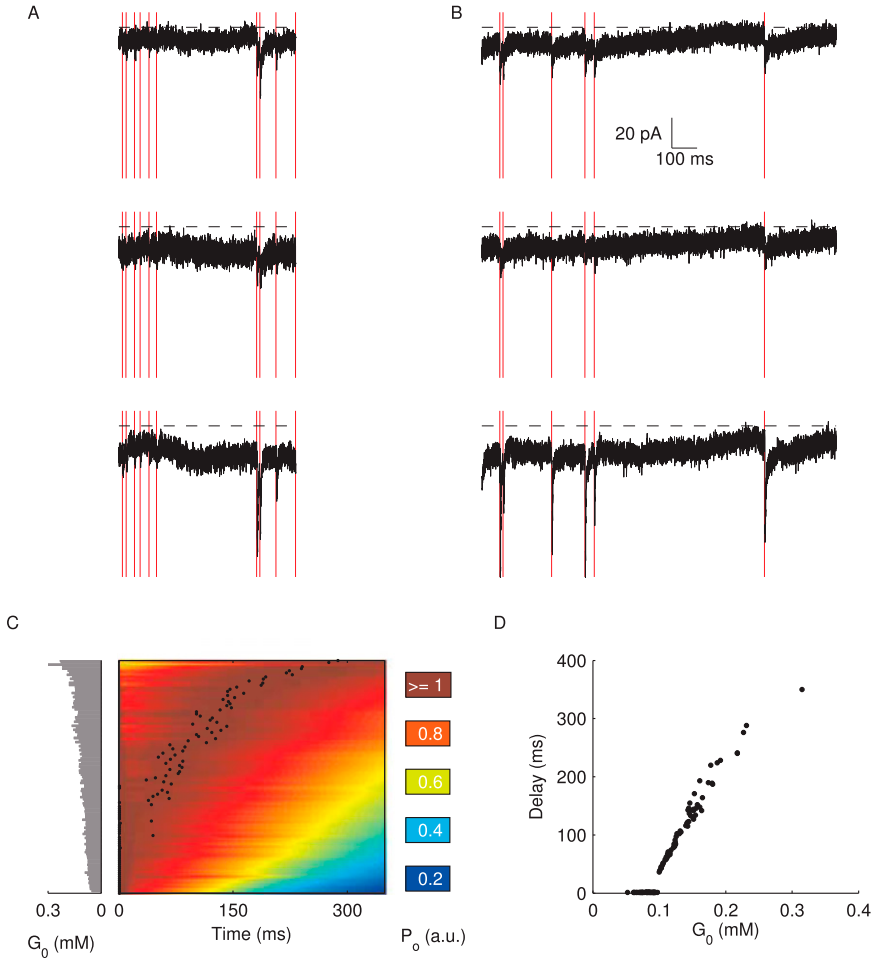

Fig. S1. Irregular stimulation. (*A*) Example traces from three different UBCs stimulated with a long-lasting irregular pattern at an average frequency of 10 Hz. As the stimulation protocol was the same for these cells, their responses could be compared. Even though these cells had different amplitudes of fast and slow EPSCs, the qualitative response to a strong stimulus burst was similar, in that a slow resurgent was generated. However, the temporal characteristics of the slow waves were different. Vertical red lines indicate stimulation times. (*B*) Example traces from three different UBCs stimulated with a long-lasting irregular pattern at 5 Hz. The lower overall stimulation frequency elicited varying response types in different UBCs. (*C*) Model simulation of AMPAR activation with the irregular stimulation patterns that were also used in experiments. The procedure for producing the heatplot is explained in Fig. 3. The model allowed to directly relate the glutamate concentration G_0 just before a stimulus to the delay of the slow EPSC. G_0 is indicated in the bar plot on the left, and the black dots indicate the peak of the slow wave in each trace. (*D*) Slow EPSC delay as a function of G_0. These model results show that G_0 encoded the slow EPSC delay during irregular stimulation trains and provide a mechanistic relation between presynaptic activity and steady-state AMPAR activation.

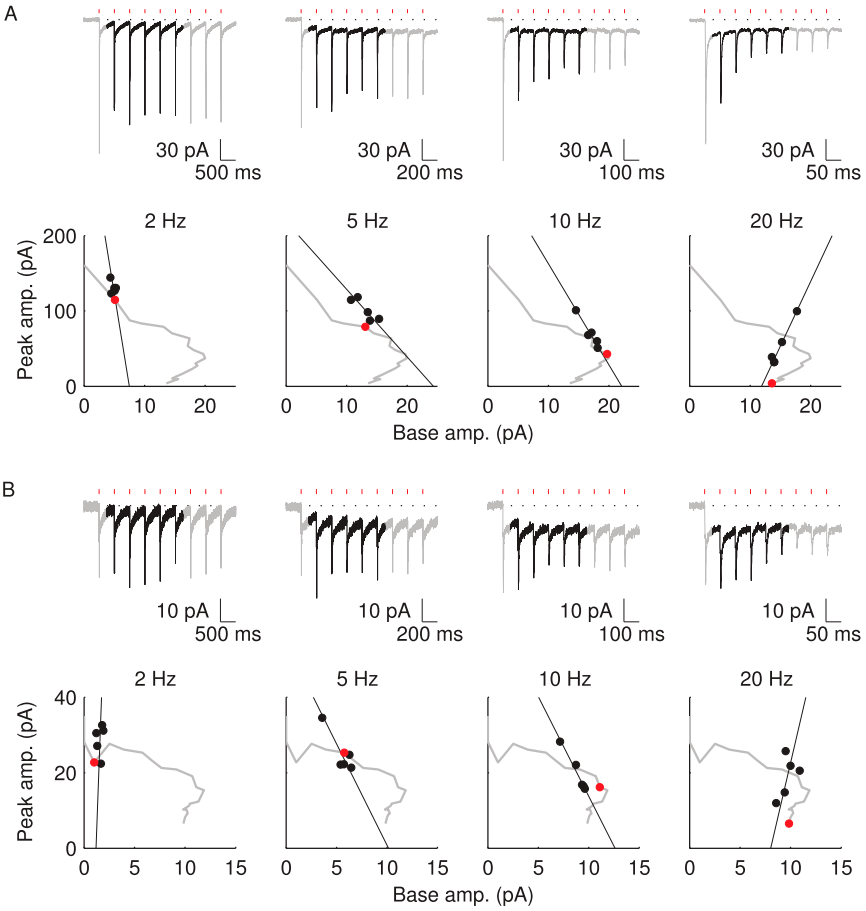

Fig. S2. Covariation of EPSC parameters. EPSC peaks are plotted as a function of corresponding baseline currents during regular stimulus trains (black dots) for two different UBCs, with a large EPSC peak (*A*) and a small EPSC peak (*B*). Adaptation occurred within the first six stimuli; the first stimulus in the train was omitted. Covariation of peak and baseline amplitudes was analyzed by comparing the two principal components; vectors corresponding to the largest components are drawn in the panels (black lines). The gray curves represent steady-state values derived from the frequency-stepping protocol described in Fig. 2; the red dots correspond to the relevant frequency in each panel. The level of coadaptation was quantified as the ratio R_λ of the eigenvalues λ of the covariance matrix, given by $R_\lambda = \lambda_{max}/(\lambda_{min} + \lambda_{max})$. The slopes S_{ad} of the adaptation vectors shifted from negative to positive values with increasing stimulation frequency; the results were as follows. 2 Hz : $S_{ad} = -7.8 \pm 14.6$ ($R_\lambda = 0.99 \pm 0.01$, $n = 7$), 5 Hz : $S_{ad} = -8.6 \pm 2.0$ ($R_\lambda = 0.95 \pm 0.03$, $n = 10$), 10 Hz : $S_{ad} = -3.0 \pm 5.5$ ($R_\lambda = 0.97 \pm 0.02$, $n = 11$), and 20 Hz : $S_{ad} = 9.6 \pm 10.5$ ($R_\lambda = 0.98 \pm 0.00$, $n = 11$).

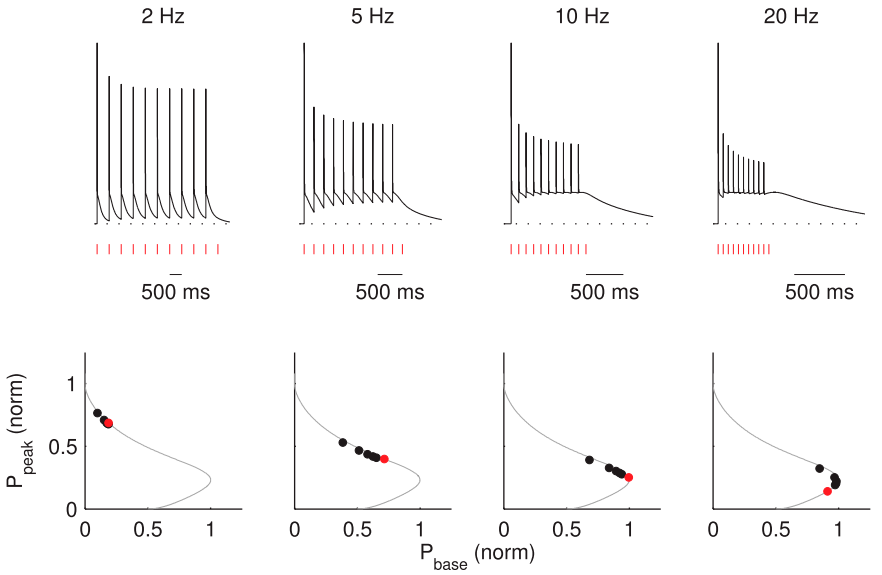

Fig. S3. Simulated regular stimulation protocol. Numerical simulation of AMPAR activation by regular stimulation trains. The glutamate model derived in the main text allowed for simulating the main qualitative characteristics of short-term adaptation to regular stimuli: strong depression of P_{peak} already at low stimulation frequencies and gradual build-up of P_{base} according to the AMPAR dose–response properties. Transient adaptation to frequencies up to 20 Hz was well described by the steady-state model, as is illustrated in the lower graphs, which display the simultaneous adaptation of P_{peak} and P_{base} on top of the steady-state curve (gray).

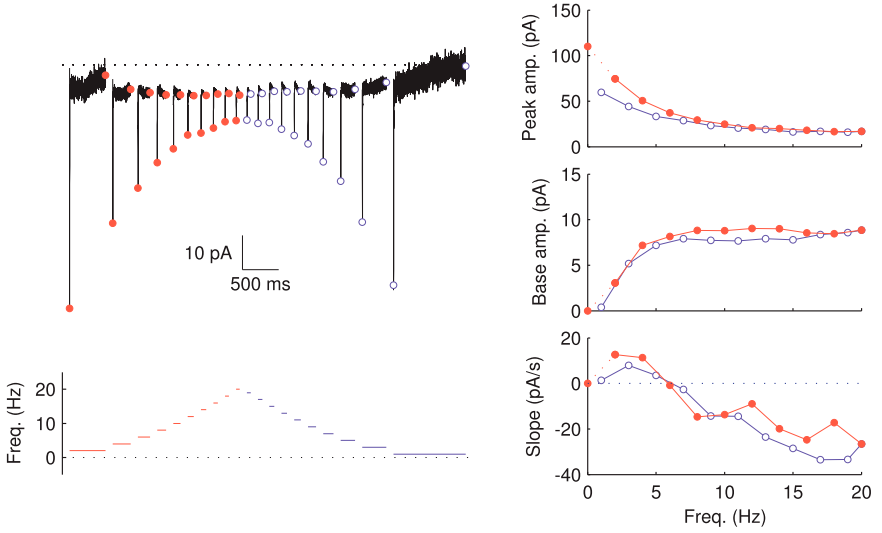

Fig. S4. Hysteresis of EPSC parameters. Example of the frequency-stepping protocol used to generate steady-state activation curves in Fig. S2 and Fig. 2. If the EPSC would be fully determined by the (quasi) steady-state activation of AMPARs, we expected that the direction of frequency stepping should not affect the resultant steady-state values, as illustrated in the simulated stepping protocol in Fig. S5. However, the EPSC peak displayed hysteresis when the stimulation frequency was stepped forward (red) and backward (blue) through the frequency range of 0–20 Hz, as shown here in the example trace. This result indicated that, apart from the steady-state process described in this work, an additional depression component gradually built up during the stimulation period, with a time constant $\gg$ 500 ms (the stimulus train lasted >100 s). This component did not affect the baseline current, however, as hysteresis was virtually absent in both baseline amplitude and slope.

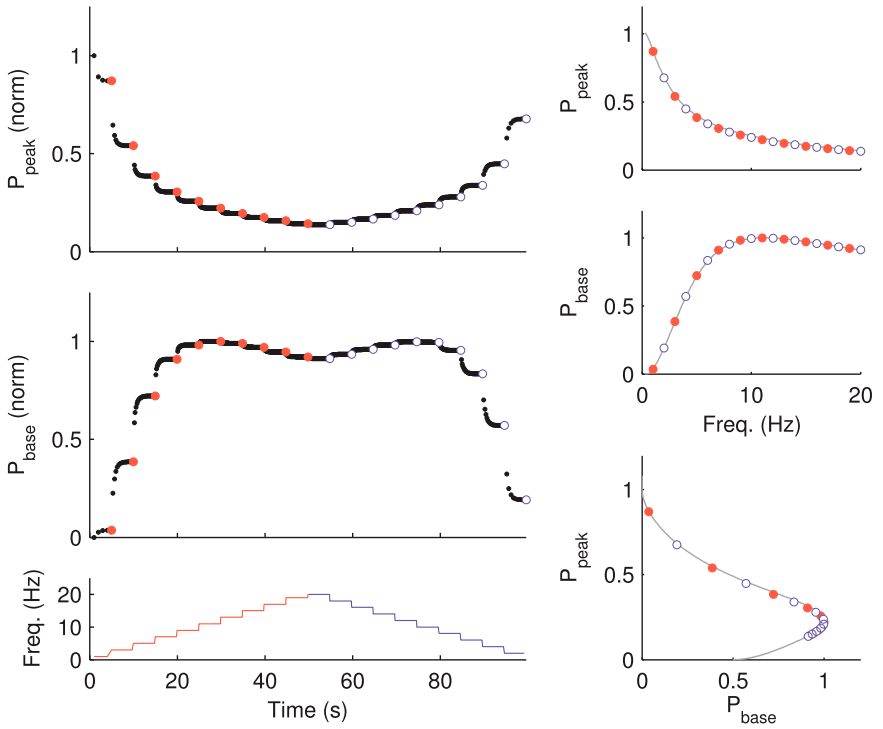

Fig. S5. Simulated frequency-stepping protocol. Numerical simulation of the frequency-stepping protocol, using the glutamate release and decay model derived in the main text (Fig. 4). In the main text, we made use of the steady-state approximation of AMPAR activation for simplicity, but we show here that the same results could be obtained by numerical integration of the full AMPAR model. As for the experimental protocol, the stimulation frequency was stepped through the range of 1–20 Hz, in 2-Hz, 5-s steps. Peak (P_{peak}) and baseline (P_{base}) open probabilities during the steps were used to generate the plots in the *Left Column*. Adaptation of these parameters largely occurred during the first second of a step, although minor adaptation continued for longer periods due to the very slow time constant (~500 ms) of glutamate removal. The values of P_{peak} and P_{base} at the end of each step were used for the plots in the *Right Column* (dots). The gray curves resulted from the steady-state approximation and matched well with the results from numerical simulation.